Supporting Information

Photochromic Control in Hybrid Perovskite Photovoltaics

Weifan Luo[1#], José María Andrés Castán[2#], Diego Mirani[2#], Antonio J. Riquelme[2], Amit Kumar Sachan[3], Olzhas Kurman,[4] SunJu Kim,[4] Fabiola Faini[5], Paul Zimmermann[6], Alexander Hinderhofer[6], Yash Patel[1], Aaron T. Frei[7], Jacques-E. Moser[7], Daniel Ramirez[8], Frank Schreiber[6], Pascale Maldivi[2], Ji-Youn Seo[4], Tress Wolfgang[3], Giulia Grancini[5], Renaud Demadrille[2], Jovana V. Milić[1*]

[1]Adolphe Merkle Institute/ University of Fribourg, 1700 Fribourg, Switzerland; [2]Université Grenoble Alpes, CEA, CNRS, Grenoble-INP, IRIG-SyMMES, 17 avenue des Martyrs, 38000 Grenoble, France; [3]Forschungsschwerpunkt Organic Electronics & Photovoltaics, ZHAW School of Engineering, 8400 Winterthur, Switzerland; [4]Department of Nanoenergy Engineering, Pusan National University, 46241 Busan, South Korea; [5]Physical Chemistry Department, University of Pavia, 27100 Pavia, Italy; [6]Institute of Applied Physics, University of Tübingen, 72076 Tübingen, Germany; [7]Photochemical Dynamic Group, Institute of Chemical Sciences and Engineering, École Polytechnique Fédérale de Lausanne, 1015 Lausanne, Switzerland; [8] Centro de Investigación, Innovación y Desarrollo de Materiales – CIDEMAT, Facultad de Ingeniería, Universidad de Antioquia UdeA, Calle 67 No. 52-21, 050010 Medellín, Colombia. [#]These authors contributed equally. [*]Corresponding e-mail: jovana.milic@unifr.ch

Table of Content

Experimental Section

Materials and Methods

Lead iodide (PbI_2, 99.99%) and cesium iodide (CsI, 99.99%) were purchased from Tokyo Chemical Industry Co., Ltd. Lead bromide ($PbBr_2$, 99.99%), formamidinium iodide (FAI, 99.8%), and methylammonium bromide (MABr, 99.8%) were purchased from Greatcell Solar Materials Pty Ltd. Spiro-OMeTAD (>99.8%) was purchased from Luminescence Technology Corp. Anhydrous *N*,*N*-dimethylformamide (DMF), chlorobenzene (CB) and dimethyl sulfoxide (DMSO) were purchased from Sigma-Aldrich Chemie GmbH.

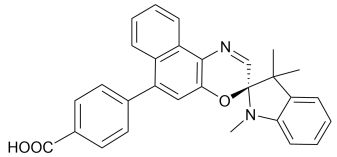

4-(1,3,3-trimethylspiro[indoline-2,3'-naphtho[2,1-b][1,4]oxazin]-6'-yl)benzoic acid (SINO) A solution of 6'-bromo-1,3,3-trimethylspiro[indoline-2,3'-naphtho[2,1-b][1,4]oxazine] (210 mg, 0.52 mmol), 4-(4,4,5,5-tetramethyl-1,3,2-dioxaborolan-2-yl)benzoic acid (122 mg, 0.49 mmol), potassium acetate (152 mg, 1.5 mmol) in a mixture of 1,4-dioxane/water (20 and 1.5 mL respectively) was degassed for 30 minutes. Then, $Pd(dppf)Cl_2$ (21 mg, 0.03 mmol) was added and the mixture was left to react at 80 °C during 16 h. Water and diethyl ether were added and then the organic layer was extracted with ether, dried with Na_2SO_4 and concentrated under reduced pressure. The resulting crude was purified by column on silica gel (eluent: from CH_2Cl_2 to CH_2Cl_2/methanol 96:4). The resulting solid was dissolved in CH_2Cl_2, then precipitated with hexane affording the expected compound by filtration as a whitish solid (82 mg, 38%). All characterisation data were consistent with those previously reported.[1]

Device fabrication involved FTO (fluorine-doped tin oxide) glass substrates that were sequentially cleaned with 2% Hellmanex solution, isopropanol, and ethanol in an ultrasonic bath for 15 min and then dried with N_2. The cleaned FTO glass substrates were then treated with UV-Ozone for 5 min prior to the deposition of TiO_2. The TiO_2 layer was deposited by aerosol spray pyrolysis using oxygen as a carrier gas. For approximately 30 samples of 1.5 x 2.5 cm (112.5 cm^2), 0.2 mL of acetylacetone and 0.3 ml of titanium diisopropoxide bis(acetylacetonate) stock solution (75 wt. % in isopropanol) is diluted in 4.5 mL of ethanol for a total of 5 ml of solution (10% conc.). Substrates are heated to 450 °C for 15 min and 30 min after the spray of the precursor solution. A layer of mesoporous TiO_2 (m-TiO_2) was deposited onto the compact TiO_2 (c-TiO_2) substrate through a spin-coating process lasting 10 se, conducted at 4000 rpm with an acceleration

rate of 1000 rpm/s. This deposition was achieved utilizing the 30NRD TiO_2 paste, with a quantity of 0.3 g per 2 mL of ethanol. Following this, the substrates dried at 100 °C, after which they underwent sintering at 450 °C for a duration of 30 min to form FTO/c-TiO_2/m-TiO_2. Subsequently, this substrate was coated with a perovskite solution that was prepared according to the method described below. For the hole-transport material, 100mg Spiro-OMeTAD was dissolved in 1.08 mL CB, doped by 23 μL Li-TFSI (1.8 mol/L in acetonitrile) and 39 μL tBP. The mixed Spiro-OMeTAD solution was spin-coated on the surface of the perovskite at 4000 rpm for 20 s with an acceleration rate of 2000 rpm/s. Finally, an 80 nm Au electrode was deposited by thermal evaporation through a shadow mask to form a device with an active area of 0.1 cm^2.[2]

Mixed cation perovskite precursor solution was prepared by dissolving a mixture of PbI_2 (543.0 mg), $PbBr_2$ (21.0 mg), FAI (189.3 mg), MABr (6.4 mg), and CsI (15.8 mg) $Cs_{0.05}FA_{0.9}MA_{0.05}Pb(I_{0.95}Br_{0.05})_3$ with 5% excess of PbI_2 in 1 mL of DMF and DMSO mixture (4:1 v/v) at 70 °C. The perovskite active layer was deposited using an antisolvent method with chlorobenzene. The perovskite precursor solution was deposited on the freshly prepared FTO/c-TiO_2/m-TiO_2 substrate, and a two-step spin-coating method was applied. The first step was carried out at 2000 rpm with an acceleration rate of 200 rpm/s for 10 s. The second step followed at 6000 rpm with an acceleration rate of 2000 rpm/s for 30 s. CB (200 μL) was slowly dripped at 15 s before the second step. After this, the substrate was annealed at 150 °C for 10 min. To treat the device, we applied a 1 mg/mL solution of SINO in toluene, which was then spin-coated on the surface at 4000 rpm for 20 s with an acceleration rate of 2000 rpm/s followed by annealing at 80 °C for 10 min.[2]

X-ray diffraction measurements were conducted using a PANalytical Empyrean Series 2. The instrument utilized Cu Kα radiation with a voltage of 40 kV and a current of 40 mA. For the specific purpose of grazing incidence measurements, the X-ray incidence angle was set at 2°. Diffracted X-rays were detected during the experiments employing a PIXcel3D detector. The chemical composition of films was measured using *XPS* (AXIS SUPRA) with an Al Ka radiation source, and all binding energies were calibrated by C 1s (248.8 eV) as a reference.

Grazing incidence wide-angle X-ray scattering (GIWAXS) was employed to analyze the thin films deposited on microscope and ITO glass substrates. GIWAXS and XRR measurements were performed at ESRF beamline BM01. The beam energy was 12.93 keV, incidence angle 0-0.6°. A PILATUS2M detector was used to record two-dimensional diffraction patterns with a sample-to-detector-distance of 640 mm.

UV-vis absorption measurements were conducted using a Shimadzu UV-2600 spectrophotometer.

Steady-state photoluminescence (PL) spectra were acquired using a Fluorolog 322 spectrometer (Horiba Jobin Yvon iHr320) equipped with a CCD detector, using a slit width of 5 nm, and the excitation by a Xenon lamp at a wavelength of 350 nm. The band slit width during the measurements was set to 5 nm.

Transient absorption measurements were performed with an ultrafast TA spectrometer (Harpia-TA, Light Conversion). A Yb:KGW laser (1030 nm, 50 kHz, Light Conversion) beam is split into two paths, where one of them is transferred to the optical parametric amplifier to generate a high intense specific wavelength for the excitation (pump) beam and the other one is focused on 5 mm of sapphire to generate a continuum light ranging from 490 nm to 900 nm employed as a probe beam. The time delays between the pump and probe light beams are traced by a motorized software-controlled delay stage. The pump and probe beams are spatially overlapped at the target samples, and the transmitted probe light is collected by an ANDOR KYMERA 193i-B2 spectrograph to calculate the differential absorption spectra.

Frequency modulated Kelvin probe force microscopy (FM-KPFM) was performed in two-pass mode using a modified AIST Omegascope AFM system. The first pass is used for revealing the morphology of the sample surface, and the V_{cpd} is determined in the second pass at the lift height of 20 nm, 1.2 V modulation voltage, and ~500 Hz modulation frequency. All the samples were scanned with Au-coated ACCESS-NC-GG AFM probes with tip radius <30 nm and resonance frequency around 270 kHz at around 0.5 Hz scan rate. Control and target samples were measured in the N_2-filled chamber with the relative humidity below 5%. Both control and target films were exposed to UV light at 40–45° angle when needed. Statistical analysis of the V_{cpd} signals over the control and the treated films was performed by analyzing multiple V_{cpd} signal images acquired at different regions of each sample, with and without UV exposed areas.

X-ray photoelectron spectroscopy (AXIS SUPRA) was performed with an Al Ka radiation source, and all binding energies were calibrated by C 1s (248.8 eV) as a reference.

Electrical impedance spectroscopy (EIS) was performed using an Autolab PGSTAT30 FRA2 potentiostat controlled by NOVA 2.1 software. The studies were conducted on complete solar cells using Thorlabs LED in a wide range of DC light intensities. The impedance spectra were obtained by applying a 10-mV sinusoidal voltage perturbation on top of a fixed bias voltage. Monochromatic red (630 nm) LED illumination to study the devices with the closed form of SINO molecules and using a white LED illumination after 15 minutes of light soaking under an AM 1.5G solar simulator to study the devices with the open form of the photochromic molecule. EIS was measured at open circuit varying the light intensity from the LED illumination. In addition, EIS under constant illumination varying the applied potential from V_{OC} to 0V was also conducted to determine the charge collection efficiency (CCE) using this expression:

$$CCE \approx 1 - \frac{R_{rec}(OC)}{R_{rec}(0V)}$$

The spectra were analyzed using ZView Software (Scribner), applying a -2RC- equivalent circuit, included as inset in Figure S15. The capacitive elements of the two RC couples is a constant phase element (CPE) instead of a pure capacitor, to account for the flat distortions of the semicircles.

Hysteresis was determined by measuring JV curves on forward and reverse bias under constant illumination from a Thorlabs LED, changing the scan rate using an Autolab PGSTAT30 FRA2 potentiostat. The illumination source was a Thorlabs LED. The protocol to study the separate effect of closed and open forms of SINO was similar to that described for impedance spectroscopy.

DFT calculations and geometry optimizations were performed by using Orca 5.0 software. The B3LYP functional associated with the D3 dispersion correction was used in all calculations. All geometry optimizations were performed with def2-svp basis sets for all atoms, while Stuttgart ECPs were used for I (28 frozen core electrons) and Pb (60 frozen core electrons). Optimizations of SINO either in closed or open form on TiO_2 or $FAPbI_3$ surface were carried out using a cluster to model the surface and freeze all cluster atoms. For this purpose, we relied on TiO_2 (anatase, 115 atoms) based on the previously reported procedure.[3] The perovskite calculations were based on the previously reported model for $FAPbI_3$ (slab = 171 atoms),[4] which was enlarged to a slab of 243 atoms to avoid edge effects when the molecule adsorbs on the cluster surface. The dipole moments of the SINO forms in their adsorption geometry were calculated with B3LYP and def2-tzvp basis sets. For TiO_2 surface we used a previously reported procedure.[3] The coordinates of the molecule were preserved to keep the orientation of the z-axis perpendicular to the surface. Results are summarized in Figure S9 and Table S1.

Supporting Data

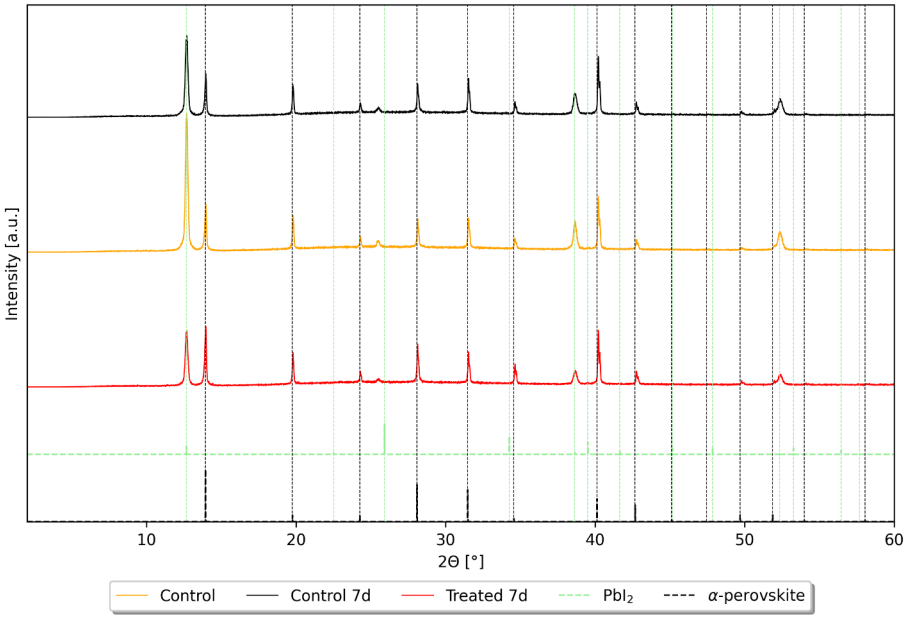

Figure S1. XRD patterns of pristine (control) and treated perovskite films with SINO (treated) after 7 days (7d) in ambient air (25 °C). The PbI_2 (green) and perovskite (black) phases are indicated by dashed lines.

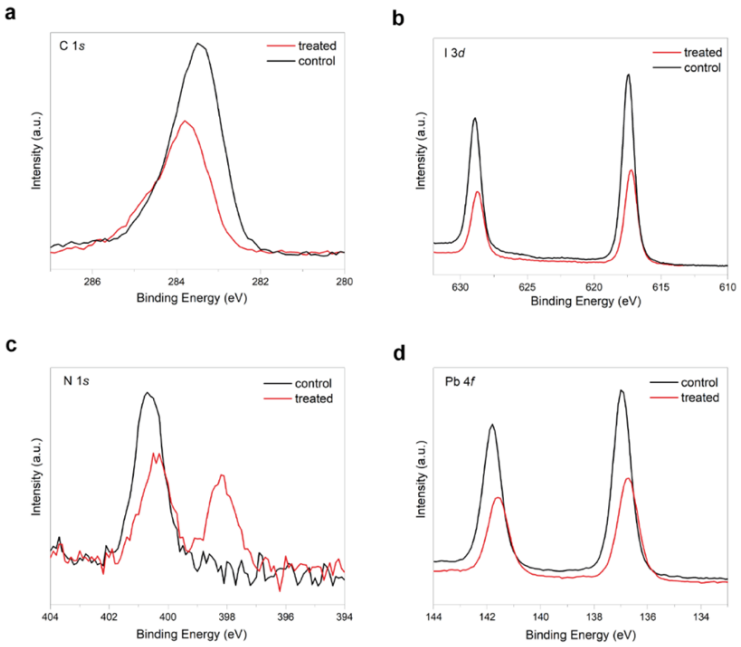

Figure S2. (a) C 1*s*, (b) I 3*d*, (c) N 1*s*, (d) Pb 4*f* XPS spectra measured on reference and SINO-treated films ($Cs_{0.05}FA_{0.9}MA_{0.05}Pb(I_{0.95}Br_{0.05})_3$).

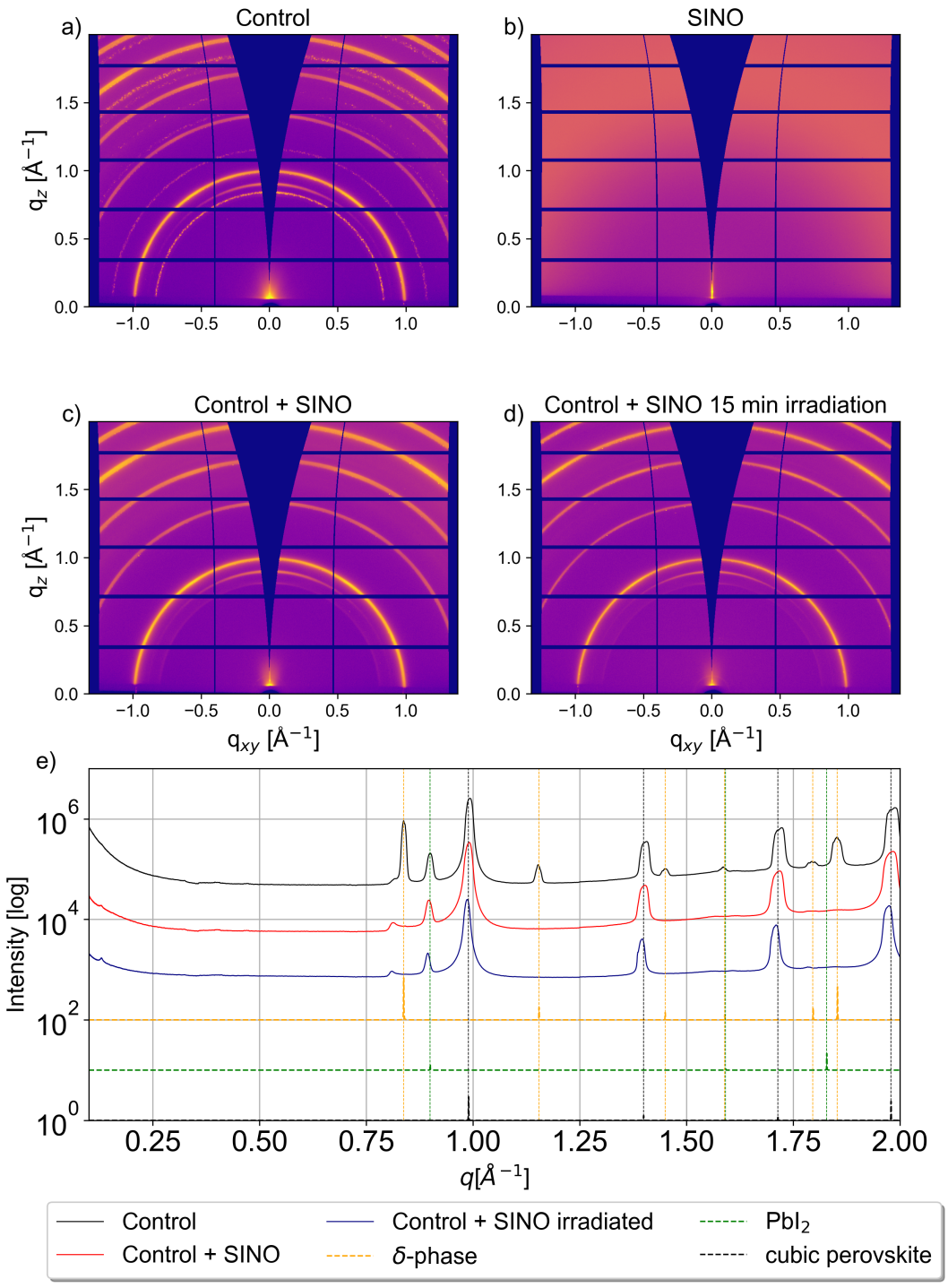

Figure S3. GIWAXS pattern, with an incidence angle of 0.6°, of (a) pristine perovskite, (b) SINO, and (c) perovskite with SINO overlayer, and (d) the GIWAXS pattern after 15 min of irradiation with a 365 nm LED lamp. (e) Radial profiles extracted from GIWAXS reciprocal space maps of the SINO-treated films and control sample. δ-phase stands for the 2H hexagonal phase.[5,6]

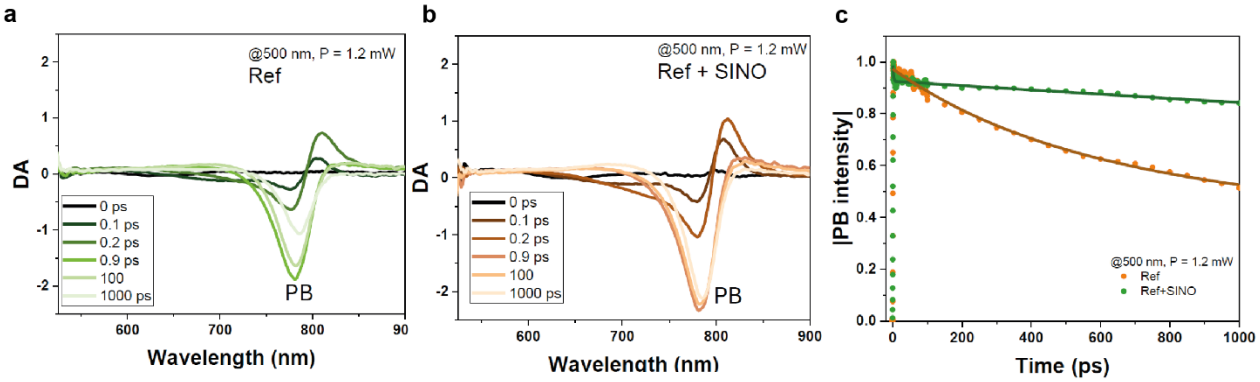

Figure S4. Transient absorption spectra of conventional triple-cation perovskite ($Cs_{0.05}FA_{0.90}MA_{0.05}$)$Pb(I_{0.95}Br_{0.05})_3$) with a 500 nm pump for (a) control and (b) treated films. (c) Charge carrier lifetime.

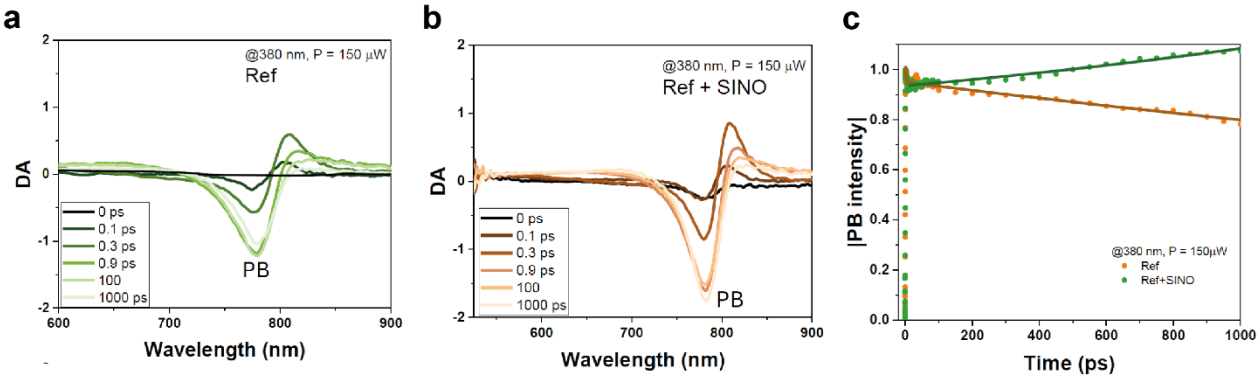

Figure S5. Transient absorption spectra of conventional triple-cation perovskite ($Cs_{0.05}FA_{0.90}MA_{0.05}$)$Pb(I_{0.95}Br_{0.05})_3$) with a 380 nm pump for (a) control and (b) treated films. (c) Charge carrier lifetime.

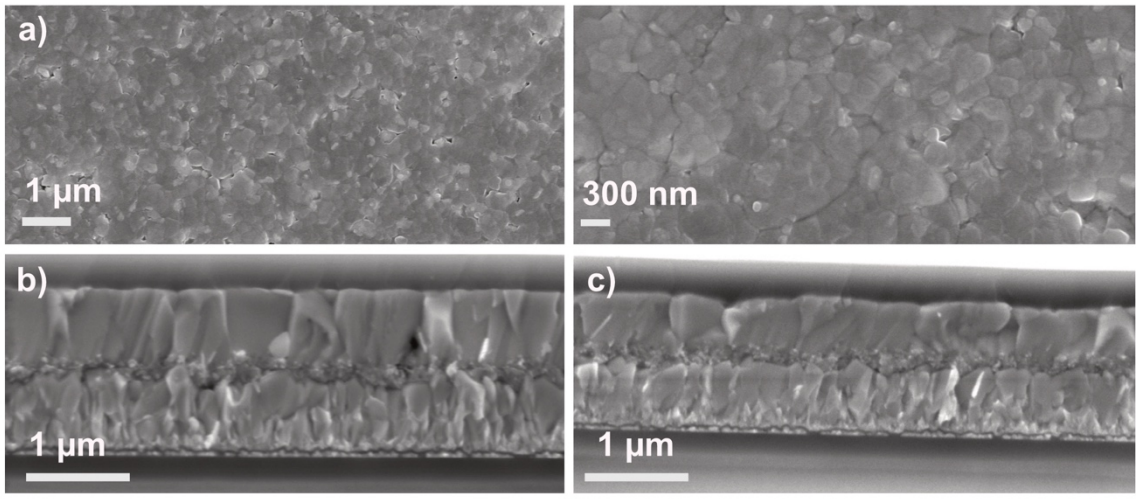

Figure S6. (a) Top and (b–c) cross-sectional scanning electron microscopy (SEM) images of control (b) and treated (a,c) perovskite (triple cation mixed halide) films (within the solar cell device) indicating the thickness of the perovskite layer of ca. 500 nm. SINO overlayer is too thin to be determined by SEM; the solution concentration allows an estimate of ca. 10–20 nm thickness.

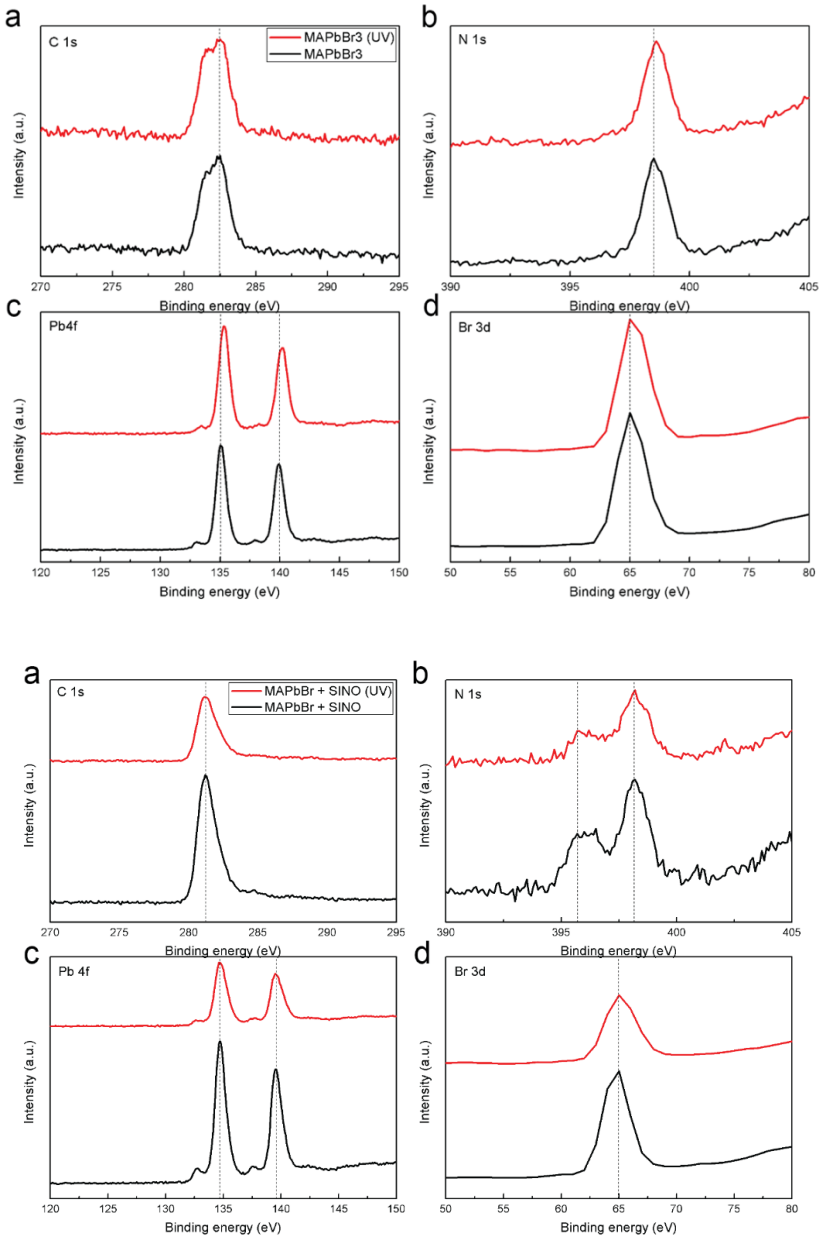

Figure S7. Top: (a) C 1*s*, (b) N 1*s*, (c) Pb 4*f* (d) Br 3*d*, XPS spectra measured on reference films ($MAPbBr_3$) with and without UV irradiation. **Bottom:** (a) C 1*s*, (b) N 1*s*, (c) Pb 4*f* (d) Br 3*d*, XPS spectra measured on reference films ($MAPbBr_3$) treated with SINO with and without UV irradiation. The differences in the spectral characteristics are the result of composition and irradiation.

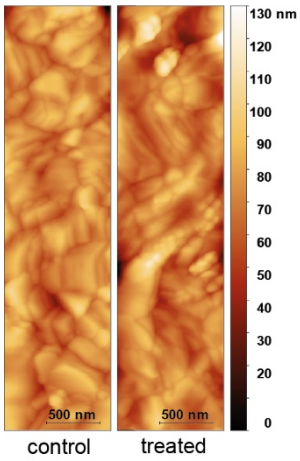

Figure S8. AFM height profile of the pristine perovskite and perovskite with SINO overlayer.

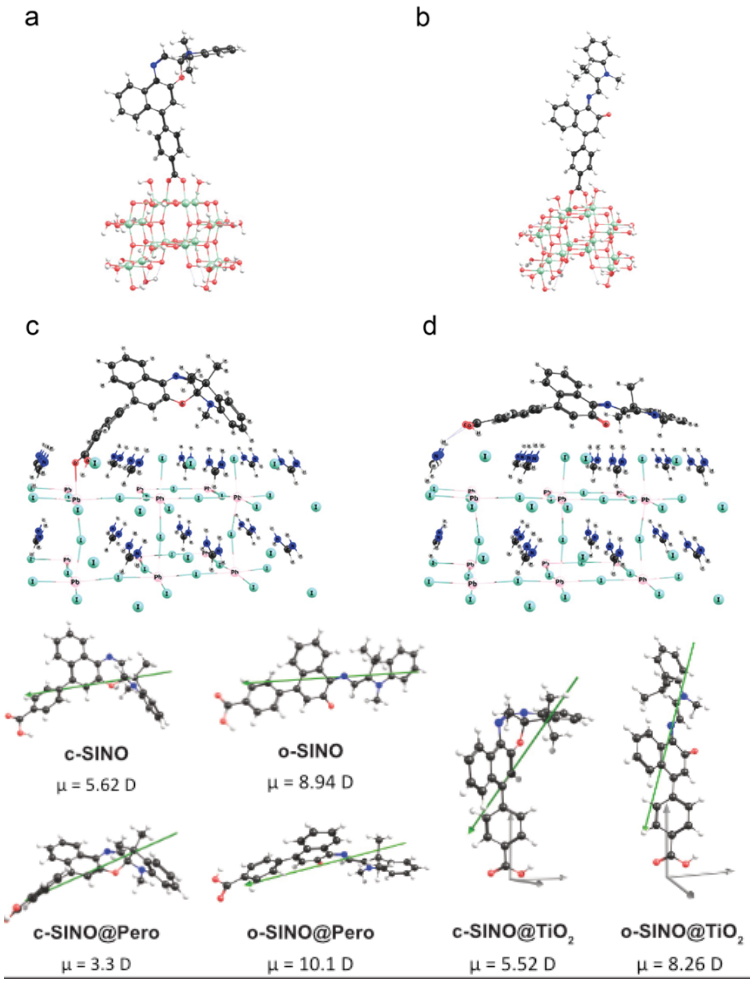

Figure S9. Top: SINO surface binding modes. (a–b) Binding on the surface of TiO_2. Deprotonation of the COOH group results in COO^- bridging on TiO_2 in the (a) closed and (b) open form of SINO. (c–d) Binding on the $FAPbI_3$ perovskite surface in the (c) closed and (d) open form of SINO. Bottom: The corresponding dipole moments (green arrows) are summarized in Table S1.

Table S1. Summary on closed (*c*) and open (*o*) forms of SINO molecular energetics and dipole moment on the TiO_2 and $FAPbI_3$ perovskite.

	c	*o*	*c*- TiO_2	*o*-TiO_2	*c*-$FAPbI_3$	*o*-$FAPbI_3$
ΔE (kcal/mol)	0	6.3	0	6.8	0	4.1
μ_{dip} (D)	5.62	8.94	5.52	8.26	3.3	10.1

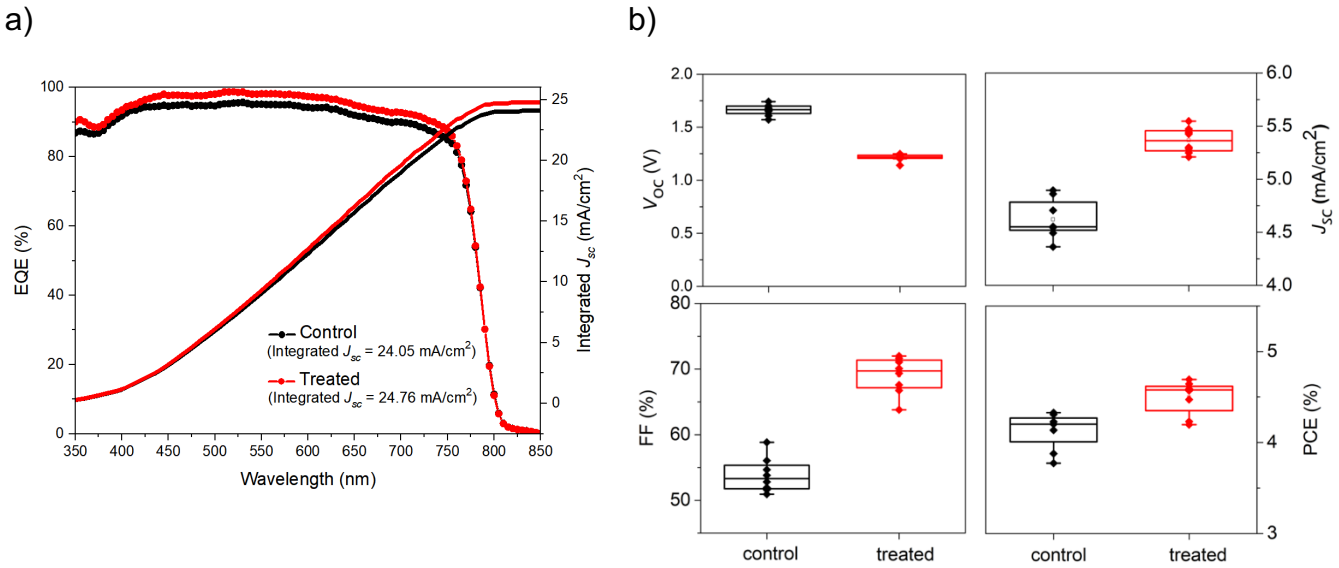

Figure S10. (a) IPCE spectra of control (black) and treated (red) solar cells. (b) Statistical distribution of open-circuit voltage (V_{OC}), short-circuit current density (J_{SC}), fill factor (FF), and power conversion efficiency (PCE) for $MAPbBr_3$-based control and treated perovskite solar cells.

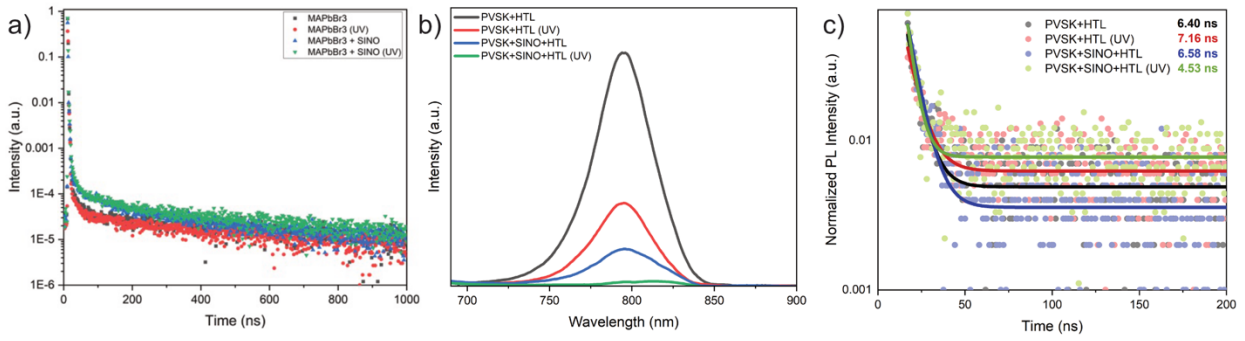

Figure S11. Time-resolved (a,c) and steady-state (b) PL spectra of (a) $MAPbBr_3$ and (b,c) triple cation double halide perovskite (PVSK) films with SINO (and HTL) before and after UV irradiation (glass side), indicating PL quenching and reduced charge-carrier lifetimes upon irradiation.

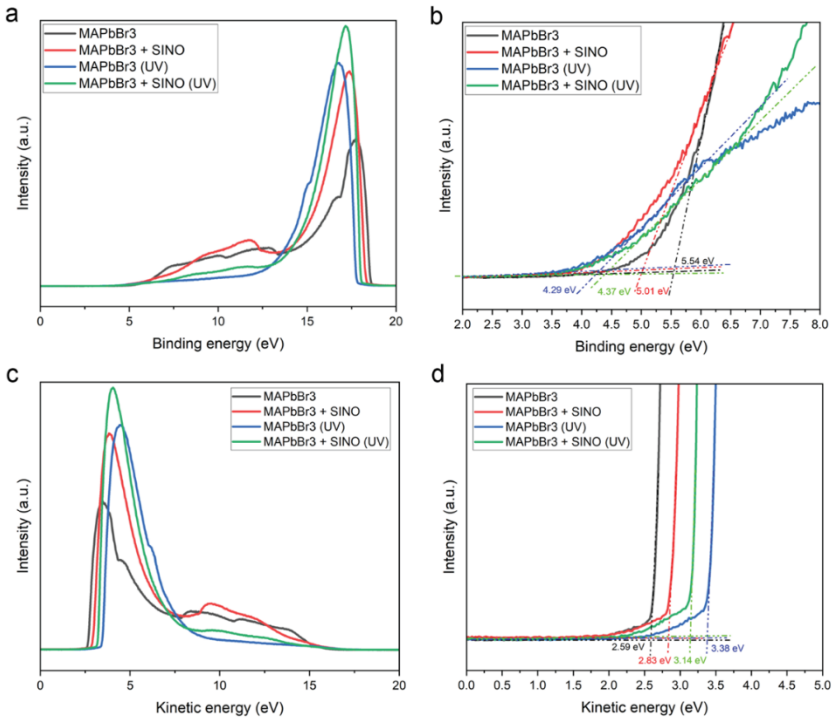

Figure S12. The UPS data of the $MAPbBr_3$ based reference perovskite film and the reference treated with SINO: (a,b) the valence band (VB) region and (c,d) the secondary electron cut-off.

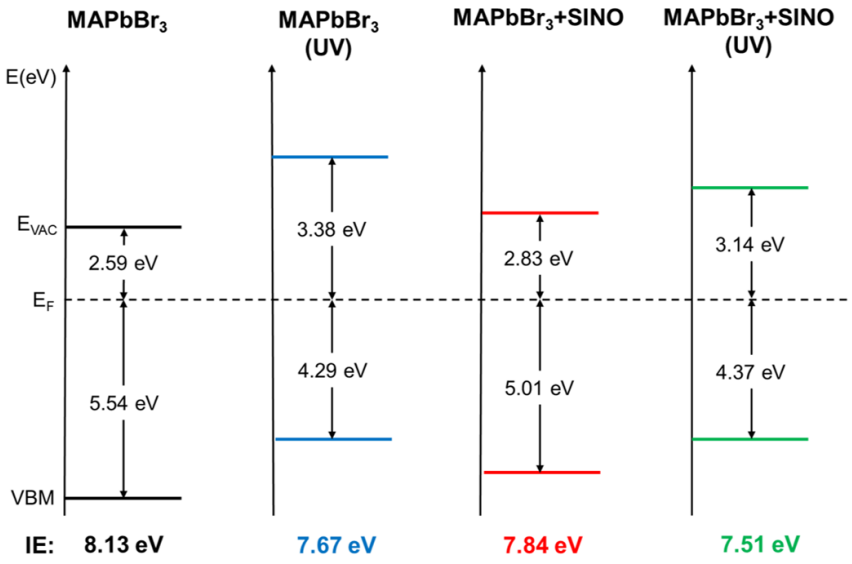

Figure S13. Energy level diagram of reference films ($MAPbBr_3$) treated with SINO with and without UV irradiation.

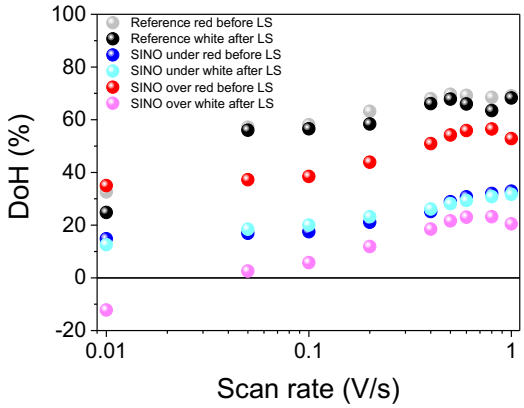

Figure S14. Value of DoH from J-V curves extracted from the photocurrent transient (forward and reversed bias) as a function of scan rate for reference devices $(Cs_{0.05}FA_{0.90}MA_{0.05})Pb(I_{0.95}Br_{0.05})_3$ and reference treated with SINO. LS corresponds to light soaking.

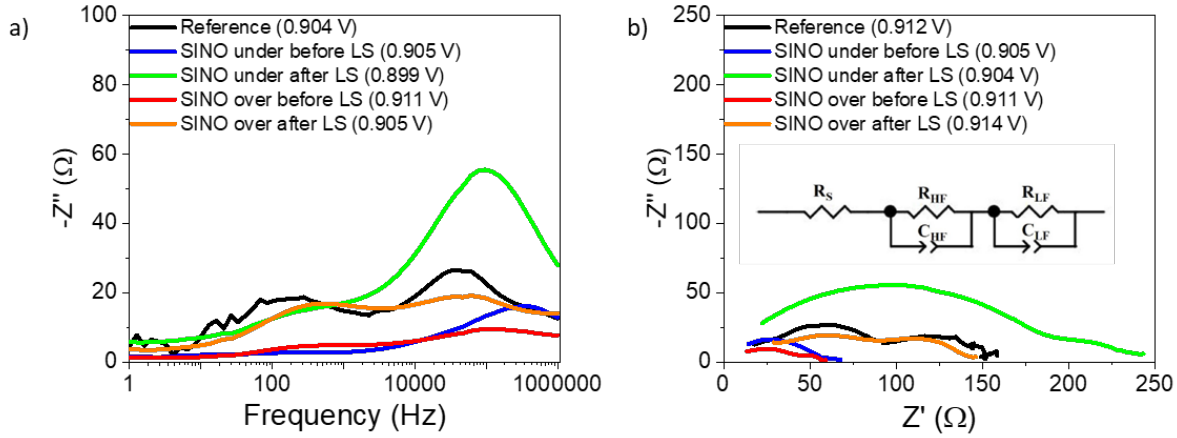

Figure S15. (a) Cole-cole and (b) Nyquist plots of electrochemical impedance spectroscopy for reference devices $(Cs_{0.05}FA_{0.90}MA_{0.05})Pb(I_{0.95}Br_{0.05})_3$ and those treated with SINO (before and after light soaking, LS). Equivalent circuit used to fit the spectra was included as inset in (b). Numerical values are shown in Table S2.

Table S2. Numerical values of recombination resistance and geometric capacitance extracted from the equivalent circuit fitting in Figure S15.

Device	Recombination resistance (Ω)	Geometric capacitance (F)
Reference	70.41	$4.95 \cdot 10^{-8}$
SINO under before light soaking	46.27	$1.07 \cdot 10^{-8}$
SINO under after light soaking	185.9	$8.51 \cdot 10^{-9}$
SINO over before light soaking	47.01	$1.93 \cdot 10^{-8}$
SINO over after light soaking	75.08	$3.41 \cdot 10^{-8}$

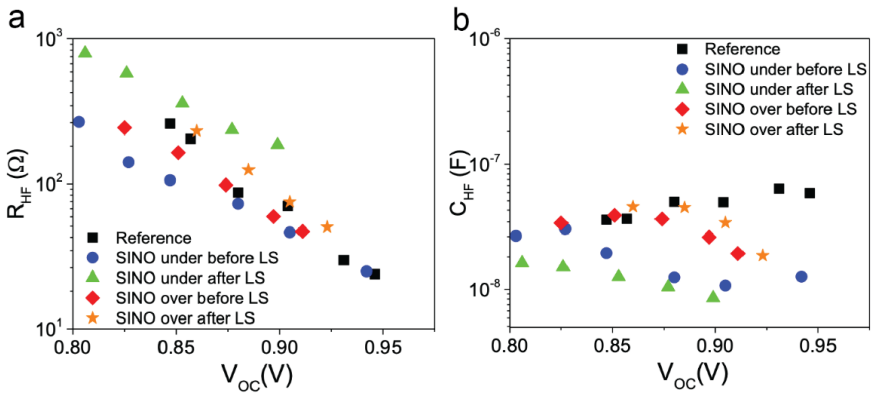

Figure S16. Impedance spectroscopy (high frequency) of reference devices ($Cs_{0.05}FA_{0.90}MA_{0.05}$)$Pb(I_{0.95}Br_{0.05})_3$) and reference treated with SINO before and after light soaking, LS). (a) High-frequency resistance and (b) high-frequency capacitance.

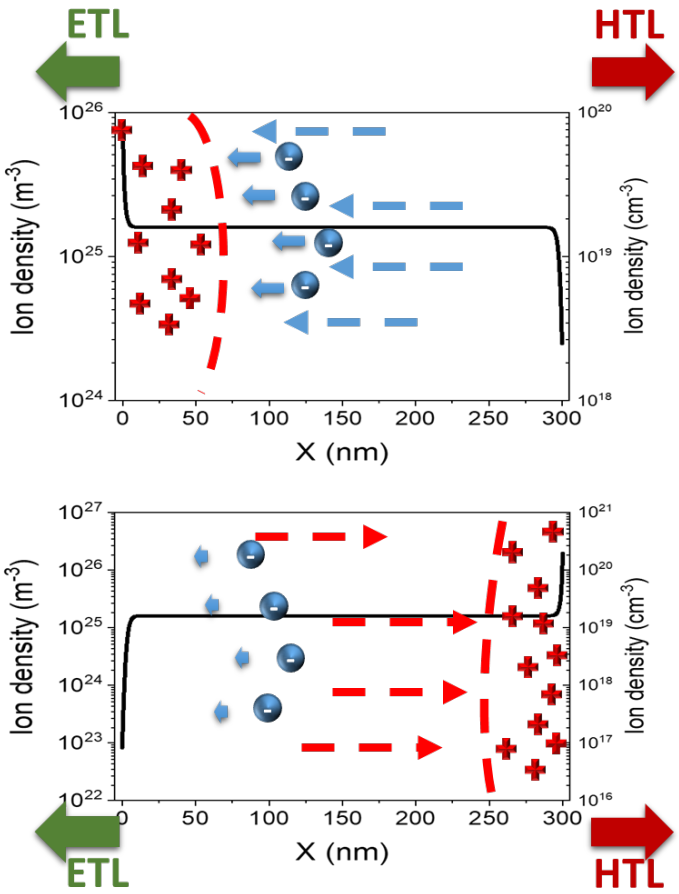

Figure S17. Schematic of the formation of Debye layers in a perovskite solar cell under conditions leading to anion vacancy accumulation in the vicinity of the ETL (top) and the HTL (bottom) and the effect of the resulting electric field on the electronic charge extraction. Red crosses represent the aforementioned ionic vacancies, the arrows the effect of the resulting electric field and blue symbols represent electronic charges.

Table S3. Estimated charge collection efficiency before and after light soaking (LS).

	Charge collection efficiency (%)
Reference	96.72
SINO at TiO_2 - before LS	92.79
SINO at TiO_2 - after LS	85.49
SINO at the HTL - before LS	96.48
SINO at the HTL - after LS	96.15

Reference

1. Andrés Castán, J.-M. *et al.* Photochromic spiro-indoline naphthoxazines and naphthopyrans in dye-sensitized solar cells. *Mater. Chem. Front.* **6**, 2994–3005 (2022).
2. Luo, W. *et al.* From Chalcogen Bonding to S–π Interactions in Hybrid Perovskite Photovoltaics. *Adv. Sci.* 2405622 (2024).
3. Huaulmamp, Q. *et al.* Photochromic dye-sensitized solar cells with light-driven adjustable optical transmission and power conversion efficiency. *Nat. Energy* **5**, 468–477 (2020).
4. Zhang, H. *et al.* Multimodal host-guest complexation for efficient and stable perovskite photovoltaics. *Nat. Commun.* **12**, 3383 (2021).
5. P. Gratia, *et al*. The many faces of mixed ion perovskites: unraveling and understanding the crystallization process. *ACS Energy Lett.* **2**, 2686–2693 (2017).
6. B Palosz. The structure of PbI_2 polytypes 2H and 4H: a study of the 2H-4H transition. J. *Phys.: Conde. Matt.*, **2,** 5285 (1990).